ATTITUDE SENSORS CALIBRATION AND MODELING FOR CUBESATS

Valdemir Carrara[(1)], Mateus Pereira[(2)], Jéssica Azevedo[(3)]
[(1)]Instituto Tecnológico de Aeronáutica (ITA) DCTA – Brazil, val.carrara@gmail.com
[(2)]Instituto Tecnológico de Aeronáutica (ITA) DCTA – Brazil, mateusop@ita.br
[(3)]Instituto Tecnológico de Aeronáutica (ITA) DCTA – Brazil, jazevedo@ita.br

***Keywords**: Attitude determination, Allan Variance, attitude sensors.*

Reliability and accuracy are critical points in a Cubesat design, mainly for the ADCS (Attitude Determination and Control System) which relies on a set composed by several sensors, actuators and electronic logic. Reliability can be achieved by redundancy if the available spacecraft internal volume and mass are not so restringing on design. Accuracy, on the other hand, can be improved by appropriate selection of sensors and by calibration. Unfortunately, laboratories with the required instruments for calibration are scarce and, normally, expensive. Calibration not only improves the pointing accuracy and stability, but also decreases the onboard control software complexity and increases fidelity of sensor models necessary for simulation. Therefore appropriate balancing of calibration costs and desired accuracy shall be carefully considered on any ADCS design. So the problem to be solved is to specify and perform some low cost calibration tests in the attitude sensors of a Cubesat. This paper describes a set of easy procedures to collect calibration data, mainly from MEMS magnetometer and gyroscopes in order to improve the model and pointing accuracy. These procedures include on ground tests using conventional EGSE or collecting data equipment like microcomputers modules, for instance, without expensive instruments. The collected data are then processed to extract sensors parameters with Allan Variance curve, which generates an accurate mathematical model of the sensor's output and noise characteristics. These strategies were applied to the ADCS sensors of SPORT Cubesat, which requires high accuracy in attitude determination, based on star sensor. However, a redundant attitude determination system based on two vectors (sun sensor and magnetometer) was employed in order to assure the required reliability when the star sensor is temporarily inactive due to sun presence in its field of view, or due to strong space radiation incidence on the CCD camera. The satellite also relies on a MEMS tri-axis gyroscope that integrates the attitude whenever the sun sensor does not give a valid measurement, when the spacecraft is in the Earth shadow, for instance. The mathematical models of SPORT sensors will be presented together with the parameters identified by the tests performed in the engineering models of sensors.

1. Introduction

Allan's Variance (AV) is a mathematical tool that was originally developed to characterize statistic errors in atomic clocks [1, 2], although it is most often used to characterize inertial sensors, such as gyroscopes and accelerometers [3, 4, 5, 6, 7, 8, 9]. This tool will be used to characterize a Invensense gyroscope MPU3300 and a magnetometer Honeywell HMC5843 that integrate the engineering model of the Nanomind (GOMSpace) computer board, that shall be employed in Cubesat SPORT for the Attitude Determination and Control Subsystem (ADCS). Several campaigns to collect gyroscope and magnetometer data were performed, with different configuration set. They were:

- Static test with both gyroscope and magnetometer running for 72 hours, with a sampling rate of 10 Hz.
- Static test with gyroscope for 3 hours at 10 Hz sampling rate, repeated five times, with complete sensor shutdown after each test.
- Static gyroscope test for 3 hours with sampling rates of 100 Hz and 250 Hz.
- Gyroscope test on a precise controlled rotation table, with 11 angular rate profiles.

The first test is intended to characterize the noise level of the gyroscope and magnetometer, in addition to their bias and stability. The second test will provide the standard deviation of the gyro's turn-on bias, while the third test aims to detect any variation in the Allan Variance curve under different sampling rate. The fourth test aims to calibrate the scale factor of the gyroscope. It should be noted that only the magnetometer's noise statistics will be characterized, since calibration requires specialized magnetic laboratory for this. Calibration tests aim to establish linearity, gain, dependence on temperature and axis alignment.

An Allan Variance curve is defined by several parameters [4]. Among them, two are relevant to the mathematical model suggested here: the angle random walk and the bias instability. The angle random walk results from noise present in the angular rate measurements, which produces a random walk when integrated in time to compute the rotation angle. The bias instability (or bias stability) results from the presence of correlated noise in the gyroscope, which changes the bias randomly (although continuously) in time. Bias instability is defined as the smallest value of the standard deviation generated in the Allan variance curve. This value depends on the set of measurements on which the standard deviation is calculated, and decreases when the number of measurements is large. However, due to bias instability, there is a limit (minimum value) from which the introduction of new measures causes the standard deviation to increase.

The reported tests were carried out with a Nanomind onboard computer of the SPORT satellite. The board comprises a microprocessor and several other circuits, in addition to an Invensense gyroscope MPU3030 and a magnetometer Honeywell HMC5843. The first experiment lasted 72 hours (approximately 3 days), and collected data from both sensors, at a rate of 10 Hz, for a total of 2592208 samples. Along with the information on the angular velocity and magnetic field in the three axes of the sensors, the temperatures from three detectors that integrate the sensors were also stored. The characterizations of the MPU3300 gyroscope and the HMC5843 magnetometer extracted from the data of the first experiment are presented in Sections 2 (gyroscope) and 3 (magnetometer).

2. Gyroscope Characterization

The statistical parameters of the gyroscope shall be compared with a mathematical model in order to allow realistic simulation of the sensors behavior. The mathematical model adopted for the gyroscope includes the effect of a dynamic bias, governed by a random walk effect. The angular velocity provided by the gyroscope model is given by

$$\boldsymbol{\omega}_g = \boldsymbol{\omega} + \mathbf{b}_g + \boldsymbol{\beta}_g + \boldsymbol{\eta}_g \,, \tag{1}$$

in which $\boldsymbol{\omega}$ is the real angular velocity, and $\boldsymbol{\eta}_g$ is a zero mean Gaussian white noise with uncorrelated standard deviation σ_η. The gyroscope bias can be separated in a

fixed bias $\boldsymbol{\beta}_g$, and a time varying bias $\mathbf{b}_g$, knew as bias instability (or stability), that can be approximated by a dynamic equation

$$\dot{\mathbf{b}}_g = \boldsymbol{\mu}_g \,, \tag{2}$$

where $\boldsymbol{\mu}_g$ is a Gaussian random variable with zero mean and standard deviation σ_μ, non correlated. The complete model incorporates also quantization and a gain, resulting in

$$\boldsymbol{\omega}_g = \frac{\text{int}\left[\left(\boldsymbol{\omega} + \mathbf{b}_g + \boldsymbol{\beta}_g + \boldsymbol{\eta}_g\right) g_{lsb}\right]}{g_{lsb}}, \tag{3}$$

where g_{lsb} = 145.6 LSB/(º/s) is the value of the gyroscope least significant bit [8], and $\text{int}(.)$ is the integer function.

The Allan Variance curve of the 72 hours static test of the gyroscope is shown in Figure 1, in units of 10^{-3} º/s. It is known that a white Gaussian noise generates a downward line in the logarithmic diagram of Allan's Variance, with a slope of $-1/2$. The bias instability introduces a correlation in the model's noise, and the random walk resulting from the bias generates a rising line with a 1/2 slope, forming a characteristic "V" shaped curve. However, real gyroscopes present diagrams that only approach the V profile, due to the presence of several correlated noise in sensor electronics. A reduction in the standard deviation associated with η causes the left arm of the V to move downwards, keeping the right arm unchanged. On the other hand, a reduction in the standard deviation in the noise associated with the bias instability, μ, displaces the right arm of V downwards, keeping the left arm in the same position. In both cases, the minimum variance, which occurs at the confluence of the two arms, changes both the frequency (x axis) and standard deviation (y axis) of the Allan Variance curve. The angle random walk (ARW) is defined by [6]:

$$\sigma_N(\tau) = \frac{N}{\sqrt{\tau}} \tag{4}$$

where N is the random angle walk (ARW), σ_N is the standard deviation associated with ARW, and τ is the time interval of the sample bin used in the composition of Allan's diagram of variance, that is, $\tau = n\,\delta t$, where δt is the sampling period and n is the number of samples contained in the bin. The random walk N can then be obtained by the standard deviation in the Allan diagram for the instant $\tau = 1$. More precisely, N is defined by the standard deviation slope line $-1/2$ tangent to the Allan's variance curve at unit value in the abscissa. It is usually expressed in º/√h, and therefore it may be necessary to convert the units of standard deviation and time. It can be noted that σ_η matches σ_N when $\tau = \tau_{sr}$, where τ_{sr} is the sampling rate considered in the model formulation.

By its turn, the bias instability B can be obtained from the expression (Hussen and Jleta, 2015):

$$\sigma_B(\tau) = \sqrt{\frac{2\ln 2}{\pi}}\, B \cong 0,664\, B \tag{5}$$

where σ_B is the standard deviation associated with bias instability, obtained by the lowest value of the standard deviation shown in the Allan Variance curve. In general, bias instability is expressed in units of º/h. Bias instability provides the smallest error that can be obtained by filtering process for angular velocity estimation. The time

associated to minimum standard deviation indicates a time constant of the gyroscope that can be used in filtering process. Although the values of σ_B and σ_μ are related, there is no explicit relationship between them.

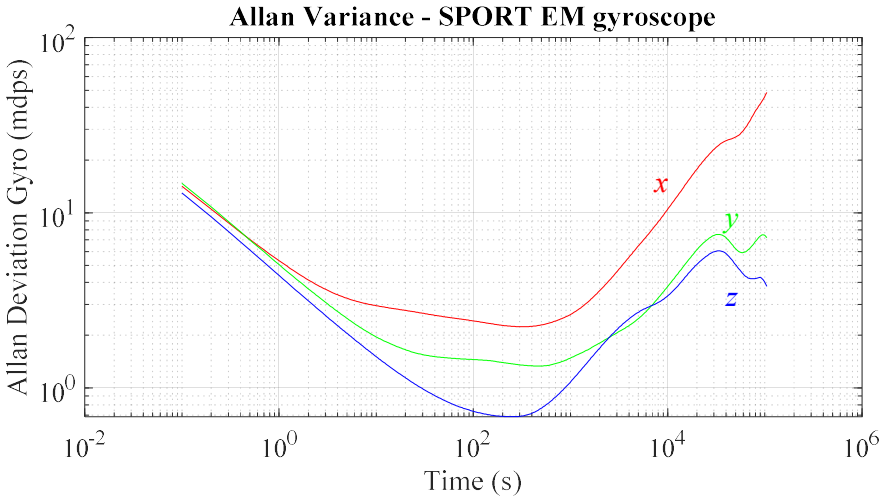

Figure 1: Allan's variance of the gyroscope.

It can be noted in Figure 1 that the gyroscope z axis tends to be more accurate than the others (lowest bias instability), probably due to the production process of MEMS sensors. Unfortunately, the Allan Variance of the mathematical model exposed in Equation 3 does not adequately fits to the data shown in Figure 1. It can fit the bias instability or the angle random walk, but not both at the same time. A more accurate model would require spectral analysis of the gyroscope noise, but the gain with such a model is small compared to its complexity. In order to produce a better adjustment of the data, the number of samples was reduced to 42000, which produces a V-profile characteristic curve of the Allan's Variance in all axes. The result of this adjustment can be seen in Figure 2, showing the curves of the gyroscope (continuous line) and model (dashed). The model was adjusted so that it is tangent to the left arm of AV and, and has the same bias instability (minimum point of the AV). The standard deviations obtained in this adjustment process were: σ_η = (13.9 14.50 13.0) 10^{-3} º/s, and σ_μ = (3.50 8.7 0.66) 10^{-3} º/s^2.

The mean value of the whole measurement set resulted in a fixed bias of β_g = (182.3 1509.3 –1501.5) 10^{-3} º/s. The measured parameters of the gyroscope resulted in a ARW of $\boldsymbol{N}$ = (0.3218 0.3092 0.2637) º/√h, a bias instability of $\boldsymbol{B}$ = (12.6832 6.8505 5.2861) º/h, and a time constant of $\boldsymbol{T}$ = (34.2 204.6 47.6) s. The large bias instability and the small time constant are the main reason of the low accuracy of MEMS gyroscopes. Although the fixed bias is high, exceeding 5000 degrees in an hour, the gyroscope error can be considered acceptable, since the fixed bias can be estimated quite accurately. The bias instability, of about 10º /h, causes the standard deviation of the bias itself to increase by 10 degrees in an hour. In the model adopted here, the bias can grow indefinitely, but in practice the bias of gyroscopes has a limit that prevents unrestricted growth [4]. The adjusted model has a ARW of $\boldsymbol{N}$ = (0.2683 0.2723 0.2469) º/√h, a bias instability of $\boldsymbol{B}$ = (12.6490 6.8530 5.3007) º/h, and a time constant of $\boldsymbol{T}$ = (7.4 34.9 39.2) s.

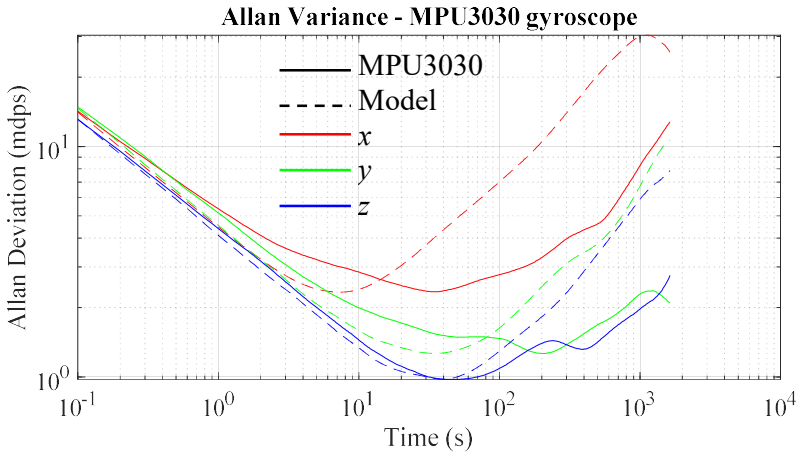

Figure 2: Allan's Variance of the gyroscope and model

The effect of the bias instability can be seen in Figure 3, which presents the bias drift calculated by a 3000 samples averaging (300 s) of the measurements, subtracted from the fixed bias β_g for each axis. Noises still present in the biases of the x and y axes practically disappear on the z axis. In this graphic is also displayed the simulated bias instability of the model, in dashed lines. It is clear that the bias instability of the mathematical model does not present the same frequency spectrum of the gyroscope, which means that the model requires further improvements.

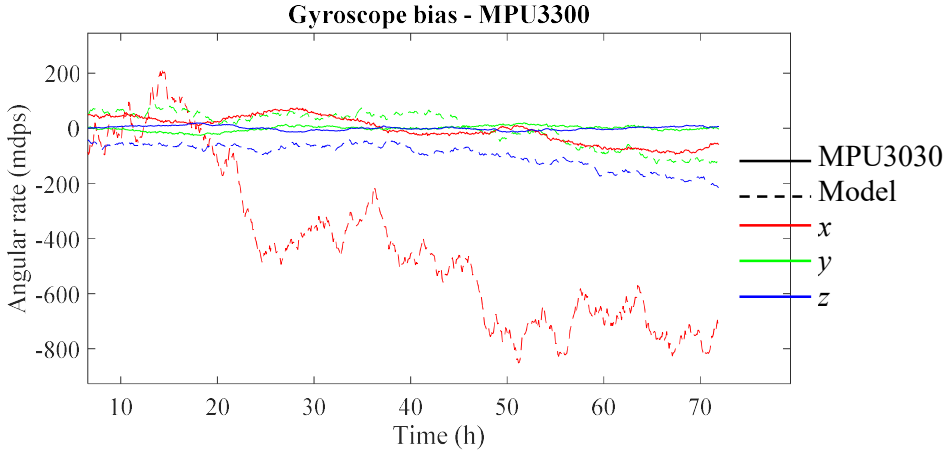

Figure 3: Dynamic bias of the gyroscope and model with an averaging of 300 s.

The second gyroscope test was performed with the sensor fixed in relation to the Earth, lasting approximately 3 hours each measurement set. This test was repeated five times, with sensor and electronics disconnected after each set, to allow changes that occur in the bias, in an effect known as turn-on bias. It was verified that there is a small bias variation at each set, when compared with the magnitude of the bias. The mean bias vector including all measurements resulted in β_g = (260.4 1490.8 −1568.4) 10^{-3} º/s, while the standard deviation vector (turn-on bias) was σ_{tob} = (23.9 11.9 14.9) 10^{-3} º/s. The turn on bias indicate the expected deviation of the bias that cannot be compensated by measurement tests.

It is expected that both the bias instability and the angle random walk decrease for high sampling rates. However, the measurements carried on the third gyroscope tests with 10 Hz, 100 Hz and 250 Hz showed that there is no reduction on

the bias instability, and the ARW had a small reduction reaching $\boldsymbol{N}$ = (0.258 0.231 0.197) º/√h, for both 100 and 250 Hz.

The fourth test consisted of sampling the gyroscope on a three-axis motion simulator. This test consisted of three sets of measurements, at an acquisition rate of 10 Hz, with each axis of the gyroscope aligned with the rotation axis of the motion simulator. The table was commanded to rotate at zero speed, 5, 10, 20, 30 and 100 º/s, in both directions, and lasting 300 seconds (5 minutes each). The Earth rotation was compensated by the motion simulator, so that the measurements are referred to an inertial system. The model adopted for calibration is linear, in the form

$$\mathbf{A}\,\boldsymbol{\omega}_g + \boldsymbol{\beta} = \boldsymbol{\omega} + \boldsymbol{\varepsilon} \tag{6}$$

where $\boldsymbol{\omega}_g$ represents the gyroscope measurement vector, $\boldsymbol{\omega}$ is the measurement vector corrected by the calibration and $\boldsymbol{\varepsilon}$ is the gyroscope error vector. Matrix $\mathbf{A}$ corrects the scale factor and cross-axis measurements, and $\boldsymbol{\beta}$ is the fixed bias vector, both being determined in the calibration process. This equation considers that the bias drift has null mean, which is approximately true for large number of samplings. The above expression can be rewritten to include the whole set of measures as

$$\begin{pmatrix} \boldsymbol{\omega}_{g1}^T & 1 \\ \vdots & \vdots \\ \boldsymbol{\omega}_{gn}^T & 1 \end{pmatrix} \begin{pmatrix} \mathbf{A}^T \\ \boldsymbol{\beta}^T \end{pmatrix} = \begin{pmatrix} \boldsymbol{\omega}_1^T \\ \vdots \\ \boldsymbol{\omega}_n^T \end{pmatrix} + \begin{pmatrix} \boldsymbol{\varepsilon}_1^T \\ \vdots \\ \boldsymbol{\varepsilon}_n^T \end{pmatrix}, \tag{7}$$

or

$$\boldsymbol{\Omega}_g\ \mathbf{B} = \boldsymbol{\Omega} + \mathbf{E}\,. \tag{8}$$

This linear regression can now be solved by least squares, which minimizes the mean square error ($\mathbf{E}^2$), and whose solution is given by:

$$\mathbf{B} = (\boldsymbol{\Omega}_g^T\ \boldsymbol{\Omega}_g)^{-1}\ \boldsymbol{\Omega}_g^T\ \boldsymbol{\Omega}\,. \tag{9}$$

which is easy to calculate, since the product in parenthesis generates a square matrix of fourth order. It was considered that the angular rate error of the three-axis motion simulator is negligible. The scale factor matrix $\mathbf{A}$ resulted in:

$$\mathbf{A} = \begin{pmatrix} 1,00330 & 0,00792 & 0,00798 \\ 0,00025 & 1,02386 & -0,01054 \\ 0,01879 & 0,00047 & 1,00042 \end{pmatrix}, \tag{10}$$

while the bias vector $\boldsymbol{\beta}$ was

$$\boldsymbol{\beta} = \begin{pmatrix} -289,59 \\ -1556,20 \\ 1627,19 \end{pmatrix}\ 10^{-3}\ \text{º/s}. \tag{11}$$

Due to the model adopted for the calibration the computed bias vector has signs contrary to that obtained previously of $\boldsymbol{\beta}_g$. The magnitudes of both, however, are quite close. The maximum error vector after calibration, given by $\mathbf{e} = \boldsymbol{\Omega} - \boldsymbol{\Omega}_g\ \mathbf{B}$, is less than 0.2% (250 10^{-3} º/s), while the error prior to calibration, $\boldsymbol{\Omega} - \boldsymbol{\Omega}_g\ (\mathbf{I}\ \ \mathbf{b})^T$, where $\mathbf{I}$ is a third order identity matrix, is 10 times larger. The gyroscope covariance matrix, given by

$$\mathrm{Cov}(\mathbf{x},\mathbf{y},\mathbf{z}) = \begin{pmatrix} E\left[(\mathbf{x}-\hat{\mathbf{x}})(\mathbf{x}-\hat{\mathbf{x}})\right] & E\left[(\mathbf{x}-\hat{\mathbf{x}})(\mathbf{y}-\hat{\mathbf{y}})\right] & E\left[(\mathbf{x}-\hat{\mathbf{x}})(\mathbf{z}-\hat{\mathbf{z}})\right] \\ E\left[(\mathbf{y}-\hat{\mathbf{y}})(\mathbf{x}-\hat{\mathbf{x}})\right] & E\left[(\mathbf{y}-\hat{\mathbf{y}})(\mathbf{y}-\hat{\mathbf{y}})\right] & E\left[(\mathbf{y}-\hat{\mathbf{y}})(\mathbf{z}-\hat{\mathbf{z}})\right] \\ E\left[(\mathbf{z}-\hat{\mathbf{z}})(\mathbf{x}-\hat{\mathbf{x}})\right] & E\left[(\mathbf{z}-\hat{\mathbf{z}})(\mathbf{y}-\hat{\mathbf{y}})\right] & E\left[(\mathbf{z}-\hat{\mathbf{z}})(\mathbf{z}-\hat{\mathbf{z}})\right] \end{pmatrix}, \tag{12}$$

where $E(\cdot)$ is the expected value (mean) of its argument, and $\hat{\mathbf{x}} = E(\mathbf{x})$ is the mean value of the $\mathbf{x}$ vector, was computed using the data available from the three-axis motion simulator test. The covariance matrix is symmetric and positive, with the squares of the standard deviation in the diagonal, and the cross variance outside the diagonal. If the measurements contained only Gaussian noise, the elements outside the diagonal would be null. The gyro's covariance matrix resulted in

$$\mathbf{G} = \mathrm{Cov}(\mathbf{x},\mathbf{y},\mathbf{z}) = \begin{pmatrix} 368{,}87 & 50{,}71 & -59{,}12 \\ 50{,}71 & 271{,}74 & -38{,}09 \\ -59{,}12 & -38{,}09 & 230{,}13 \end{pmatrix} 10^{-6}\ \mathrm{deg}^2/\mathrm{s}^2, \tag{13}$$

which indicates that the standard deviations in the axes are between 15 and 20 10^{-3} º/s.

3. Magnetometer Characterization

Nanomind uses a Honeywell HMC5843 magnetometer, which employs magneto-resistive technology incorporated into a silicon wafer. Magnetometers are usually accurate instruments, reaching up to one part per billion. On the other hand, the terrestrial magnetic field is easily distorted by the presence of magnetic materials, such as steel, iron, or by electric currents in the vicinity of the magnetometer, thus making the measurement less reliable, and thereby reducing the accuracy of the sensor. The distortion of the terrestrial magnetic field introduces a bias in the measurements of the magnetometer. The disturbance may have an internal origin that is induced by the sensor itself, or it may have an external cause. In addition, all types of biases contain a constant term and one that varies over time, with different causes. The external bias is indistinguishable from the Earth's own magnetic field, and therefore impossible to detect or measure. The other biases can be measured using special techniques for filtering the sampling data.

Computational models of magnetometers generally incorporate Gaussian noise and a constant bias. However, the Allan Variance analysis of the magnetometer had shown that the bias cannot be considered constant, but varies in the form of a random path, similarly to a gyroscope bias. In order to have a good accuracy in determining the attitude, the bias of a magnetometer needs to be estimated with high reliability.

The bias random walk (which is equivalent of the angle random walk of the gyroscope) can be modeled analogously to the gyroscope bias, described in the previous section. As with the gyroscope, the model does not restrict bias, which means that it can grow in an uncontrolled way, which does not happen in reality (Woodman, 2007). As a result, a model with a constant bias cannot reproduce the dynamics present in the sensor bias, while a model that considers variation in the bias tends to present discrepant errors over time. Each model has its own pro and cons, and shall be selected according to the end application.

The magnetometer manufacturer reports that the sensitivity of the sensor is 1300 counts/mGauss (milli Gauss), for a scale of 1 Gauss, which is the default

setting of the sensor. However, measurements indicated that this information is incorrect, and the conversion factor is actually 1.3 LSB/mGauss. The adopted mathematical model for the magnetometer is similar to the gyroscope model, given by

$$\mathbf{B}_m = \mathbf{B} + \mathbf{b}_m + \boldsymbol{\eta}_m , \tag{14}$$

where $\mathbf{B}$ is the vector of the terrestrial magnetic field, $\mathbf{b}_m$ is the sensor bias, and $\boldsymbol{\eta}_m$ is a zero mean Gaussian white noise with standard deviation of $\boldsymbol{\sigma}_\eta$, not correlated. Analogous to the gyroscope, the bias vector also presents a variation that can be modeled as

$$\dot{\mathbf{b}}_m = \boldsymbol{\mu}_m , \tag{15}$$

in which $\boldsymbol{\mu}_m$ is a white Gaussian noise with $\boldsymbol{\sigma}_\mu$ standard deviation. The final expression for the magnetometer model, considering the gain and quantization is

$$\mathbf{B}_m = \frac{\text{int}\left[\left(\mathbf{B} + \mathbf{b}_{m,k} + \boldsymbol{\eta}_m\right) m_{lsb}\right]}{m_{lsb}} , \tag{16}$$

and m_{lsb} = 1.30 LSB/mGauss is the sensor gain. Figure 4 shows Allan's Variance curves of the magnetometer, for the 72 hours duration measurements. It can be noted the strong presence of white Gaussian noise in the decreasing part of the curves, with a slope very close to –1/2. The bias instability can also be seen in the figure, with a time constant of approximately 20 minutes in all axes. The adjustment of Allan's variance curves to the mathematical model is shown also in Figure 4, in dashed lines. The model fitted very well to Allan's variance diagram, even reproducing accurately the bias instability. The standard deviations obtained from the Allan's Variance analysis are, in vector form, $\boldsymbol{\sigma}_\eta$ = (3.0 4.9 2.96) mGauss and $\boldsymbol{\sigma}_\mu$ = (0.0034 0.0042 0.0036) mGauss/s resulting in a random walk of $\boldsymbol{N}$ = (0.01568 0.02587 0.01588) mGauss√h and $\boldsymbol{B}$ = (0.05376 0.07180 0.04988) mGauss. The time constant of the magnetometer is $\boldsymbol{T}$ = (1132.3 1414.1 1265.4) s.

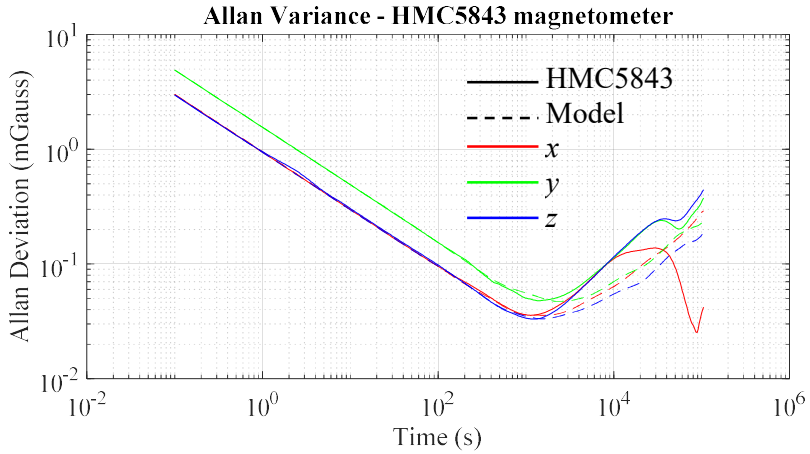

Figure 4: Allan Variances of the magnetometer and mathematical model.

The magnetometer bias is shown in Figure 5, for both the measurement set and model, extracted from an average of one thousand seconds (10k samples), subtracted from the mean value of each axis. This figure shows a periodic behavior of the measurements in all axes, with frequency of one cycle per day. This behavior

is undoubtedly associated with the temperature variation during measurements, and was not considered in the model. The local temperature, sampled also with the magnetic field, shows also a periodic variation, ranging from 25 up to 28 °C. This clearly indicates that the magnetometer bias is dependent of temperature, at an approximate rate of 0.7 mGauss/°C. The presence of noise with similar statistic in the bias curves of magnetometer and model, attests that the model represents the sensor in a satisfactory way. It should also be noted the small magnitude of the bias variation (about 0.1% of the full scale), which attests to a good stability of the measurements.

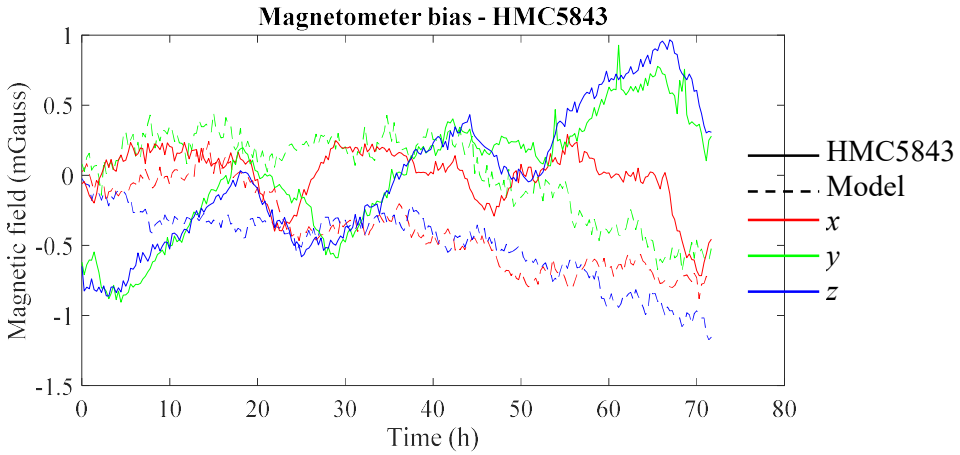

Figure 5: Bias evolution of the magnetometer and the mathematical model.

The covariance matrix of the magnetometer was calculated based on the first 13000 measurement, which correspond approximately to the sensor's time constant. Unlike the gyroscope, the elements off diagonal indicate the influence of noise coming from electrical, magnetic and temperature effects, but does not necessarily imply in misalignment of axes. The covariance matrix of the magnetometer resulted in

$$\mathbf{G} = \mathrm{Cov}(\mathbf{x},\mathbf{y},\mathbf{z}) = \begin{pmatrix} 8,6351 & -0,0087 & 0,2347 \\ -0,0087 & 6,7482 & 0,1605 \\ 0,2347 & 0,1605 & 8,6636 \end{pmatrix}, \tag{17}$$

It is noticed that the magnetometer has a covariance close to a diagonal matrix, which proves a small correlation between the axes.

4. Conclusions

The calculated parameters of the gyroscope had a good adjustment to the experimental data, except for the time constant on the x axis. The reason is the anomalous behavior of Allan's variance on this axis, probably caused by correlated noise. The bias of the gyroscope model does not fully fit the measurements, which indicates the presence of more complex noise pattern in the MPU3030. Moreover, since the model's bias is not confined to a range of angular velocities, it may exhibit a simulated measure significantly different from the gyroscope, which increases the integrated error. Therefore, the gyroscope's behavior should be expected to be better than that shown in the model.

The magnetometer model has shown a good agreement with the experimental values, both in high and low frequencies present in the signal. This ensures high fidelity of the model during attitude simulation and control tuning. However, long-running simulations can present discrepancies in relation to the magnetometer, since the magnetometer bias remains confined around the magnetic field, while the model bias can drift indefinitely, although with low probability of occurrence. A magnetic clean room with calibrated magnetic instruments and a large 3-axis Helmholtz coil is necessary to properly calibrate the satellite magnetometer. However, such laboratory is not easily accessible for Cubesats due to the high cost of calibration process. Moreover, it is expected that the satellite magnetic moment varies with time, as well as with switching of onboard instruments, which affects the magnetometer bias. A simple calibration routine based on measurements at several orientation of the satellite will be done prior launching in order to estimate the magnetometer bias. Several methods and algorithms can be employed to perform such estimates, as, for instance, the TWOSTEP [11].

References

[1] Allan, D. W. Statistics of Atomic Frequency Standards, Proceedings of IEEE, Vol. 54, No. 2, pp. 221-230, Feb, 1966.

[2] Allan, DW, Time and Frequency (Time-Domain) Characterization, Estimation, and Prediction of Precision Clocks and Oscillators ", IEEE Transportations on Ultrasonics, Ferroelectrics, and Frequency Control, Vol. UFFC-34, no.6, pp.647- 654, 1987.

[3] A Freescale Semiconductor. Allan Variance: Noise Analysis for Gyroscopes. Application Note, No. AN5087, Rev. 0, 2015.

[4] Woodman, O. An introduction to inertial navigation. University of Cambridge. Technical Report No. 696 - UCAM-CL-TR-696. ISSN 1476-2986, 2007.

[5] Hou, H. Modeling Inertial Sensor Errors Using Allan Variance. Thesis. University of Calgary. UCGE Reports No. 20201, 2004.

[6] Hussen, A. A .; Jleta, I. N. Low-Cost Inertial Sensors Modeling Using Allan Variance. International Journal of Electrical and Computer Engineering. Vol. 9 No. 5, 2015.

[7] Lam, Q. M .; Stamatakos, N .; Woodruff, C .; Ashton, S. Gyro Modeling and Estimation of Its Random Noise Sources. AIAA Guidance, Navigation and Control Conference and Exhibit, 2003, Austin, Texas. AIAA-2003-5562. 2003.

[8] Pupo, L. B. Characterization of Errors and Noises in MEMS Inertial Sensors Using Allan Variance Method. Thesis. Universitat Politècnica de Catalunya. 2016.

[9] Wang, L .; Zhang, C .; Gao, S .; Wang, T .; Lin, T .; Li, X. Application of Fast Dynamic Allan Variance for the Characterization of FOGs-Based Measurement While Drilling. Sensors, Vol. 16. No. 2078, doi: 10.3390 / s16122078, 2016.

[10] Invensense, MPU-3300 Product Specification (Revision 1.1). Invensense Inc. Datasheet. 2011.

[11] Alonso, R.; Shuster, M. D. TWOSTEP: A Fast Robust Algorithm for Attitude-Independent Magnetometer-Bias Determination. The Journal of the Astronautical Sciences, Vol. 50. No. 4, Oct-Dec 2002, pp 433-451.